Chapter

Plastic Deformation Behavior in Steels during Metal Forming Processes: A Review

Sanjeev Kumar and Erwin Povoden-Karadeniz

Abstract

The plastic deformation occurs in steels during metal forming processing such as rolling, forging, high-pressure torsion, etc. which modify mechanical properties of materials through the grain refinement, and the shape change of objects. Several phenomena in the scope of plastic deformation, such as hardening, recovery, and recrystallization are of great importance in designing thermomechanical processing. During the last decades, a focus of research groups has been devoted particularly to the field of metals processing of steel parts through plastic deformation combined with specific heat treatment conditions. In this review chapter, the current status of research work on the role of plastic deformation during manufacturing is illuminated.

Keywords: Plasticity, Ferrous metal, steel, SPD, Deformation, Strengthening, Flow Curves

1. Introduction

In the modern era, the demand for lightweight material products is being increased in industries e.g. aerospace [1, 2], automobiles [3, 4], buildings [5, 6], trains [7, 8], forged connecting rods and pistons [9], bridges [10], naval [11–13], etc. for a high living standard (see **Figure 1**). The researchers are dedicating high effort to increase the strength to weight ratio by grain refinement through applying heat treatments [14–20], mechanical processing [21, 22], and a combination of both i.e. thermomechanical processing (TMP) [23–27]. TMP methods are being used in the manufacturing unit to fulfill requirements of grain refinement of materials and create optimum semi-finished and finished products for the applications. The grain size of steels is an important factor that affects all aspects of the mechanical, chemical, and physical behavior of metals to the surrounding media. It is well known that the smaller grains support an increase in grain boundaries in the matrix. In particular, according to the Hall-patch law, the reduction in grain size improves material properties like strength Eq. (1), hardness, and impact toughness except for the ductility of steels [28].

$$\sigma_Y = \sigma_i + K_Y / \sqrt{D} \tag{1}$$

Where: σ_i = friction stress, D = grain diameter, K_Y = yield coefficient or "locking parameter" that shows the relative hardening contribution of grain boundaries.

Figure 1.
Some important examples of industrial applications which developed using metal forming processes.

Some of the major metal processing steps are often involved such as rolling, forging methods with wide temperature ranges (cold, warm and hot deformation temperature ranges) for the grain refinements [26, 27, 29–32]. The high-pressure torsion, equal channel angular pressing (ECAP), direct/indirect extrusion methods etc. are being used for ultrafine grains in which plastic transformation reaches over strain 1 through severe plastic deformation (SPD) [33–35]. In this SPD processes, the large shear stress involved usually results in a complex stress state resulting in a high defect density and homogeneous ultrafine grains.

During metal forming processing, the steel experiences different metallurgical phenomena like work hardening, dynamic recovery, dynamic recrystallization, flow instabilities, etc. [32, 36–38]. The effect of these metallurgical phenomena can be understood through the interpretation of flow curves [26, 31, 39, 40]. Where, the flow stress dependent on various processing parameters such as temperature, strain rate, and strain, etc. that can typically been described via constitutive equation.

This chapter focuses on plastic deformation behavior which can be controlled through processing parameters that affect microstructure refinement and associated mechanical properties of metals and steels during forming.

2. Some common metal processing and joining setups

A schematic diagram of rolling, forging, and high-pressure torsion (HPT) is shown in **Figure 2**. These represent basic processes within metals engineering, which change the shape and microstructure through plastic deformation for different products and applications. **Figure 2a** illustrates the rolling process setup, where the billet is pulled out between pairs of rollers which reduce the thickness of plates and grain size as well as defects like porosity and inclusions of the billet. The resulting refined grains are found to be elongated along the longitudinal direction. In the forging process, the force is imposed on objects either by hammer and anvil or in a large forging tool (called drop hammer) which results in desired and controlled shape changes (**Figure 2b**). Eventually, the HPT setup is one kind of torsion process in

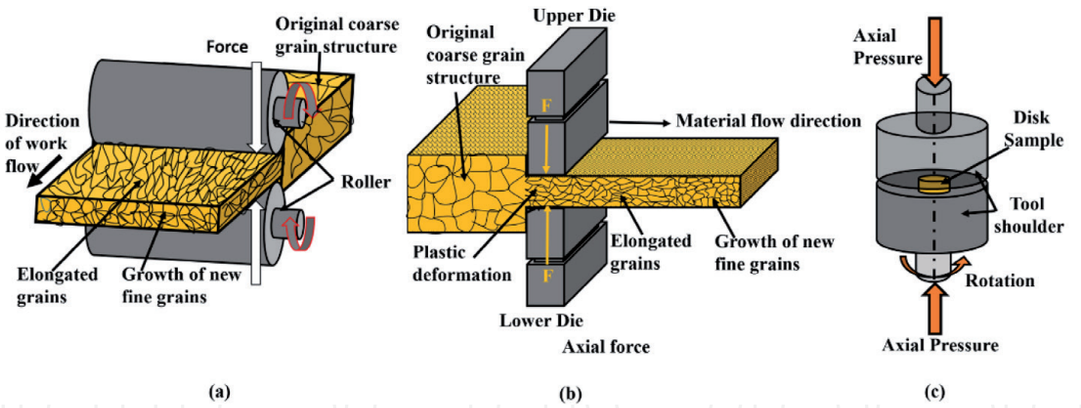

Figure 2.
Schematic diagram of metal forming processes (a) forging, (b) rolling, (c) high-pressure torsion [41].

Hot compression testing	
Strain rate (1/s)	**Machine details**
10^{-3} to <5	Basic unit, Gleeble
10^{-2} to 100 <$3x10^{2}$	Hydrawedge unit standard specimen ϕ10 x L15 mm modified specimen ϕ10 x L0.5 mm
0.1 to $5x10^{2}$	Cam Plastometer and Drop Test
$2x10^{2}$ to 10^{4}	Split Hopkinson Pressure Bar
10^{3} to 10^{5}	Taylor impact machine
More than 105	Gas gun (single & two-stage)
Torsion/Multiaxial/Shear testing	
<10^{-1}	Conventional shear machine
10^{-1} to 10^{2}	Hydrawedge unit, Gleeble
10^{-1} to 10^{3}	Torsion unit, Gleeble
10^{2} to 10^{4}	Split Hopkinson Pressure Bar
10^{3} to 10^{4}	Double-notch Shear and Punch
10^{4} to 10^{7}	Pressure-shear plate impact machine

Table 1.
Wide range of hot compression test setups [42].

which material undergoes severe plastic deformation via applying both compressive force and twisting action concurrently under high pressure (**Figure 2c**). The sample for SPD is located between two anvils, where the top anvil provides a compressive force on the sample while the bottom side anvil rotates along on axis. This setup generates shear strains in the object which are responsible for the development of ultrafine grains. Therefore these setups can be supportive of favorable mechanical properties and good product performance.

Important experimental machines, being used for a wide range of strain rates are listed in **Table 1**. In this list, the Gleeble machine can be used for axial compression testing with the strain rate between 0.001 to 100 for standard samples with a diameter of 10 mm and a length of 15 mm. It should be noted that much higher strain rates up to 3000 are feasible when a shorter sample, typically less than 1 mm, is chosen. A wide range of strain rates can be achieved using other compression testing machines, Cam plastometer, Slip Hopkin, Taylor, and gas gun machine.

Some important torsion test setups are listed for shear testing with a wide range of strain rates within the framework of SPD. All of the listed setups are supportive for controlled and taylored TMP in order to achieve an optimized balance of processing costs, time, and materials properties for various industrial applications.

3. A basic understanding of microstructure

The morphology of materials can be defined through shape, size, and structure that plays an important role in both mechanical and corrosion resistance properties. It is well known that all materials are composed of atoms that are arranged in short/long-range order with regular/irregular patterns, those solids are familiar as crystalline and non-crystalline, respectively. The crystalline metals with different crystal structures, such as body-centered cubic, face-centered cubic, or hexagonally closed packed, are prorated into the single crystal and polycrystalline categories. Conversely, most polycrystalline metals are composed of a collection of many small single crystals named grains and are similar to pomegranate fruit, which is made up of many small seeds (see **Figure 3a**). The grains are separated from each other by grain boundaries while preserving the integrity of the metal. Similarly **Figure 3b** shows one grain (shown by yellow dotted line) that has a subgroup of several laths, and every lath having several crystal atoms.

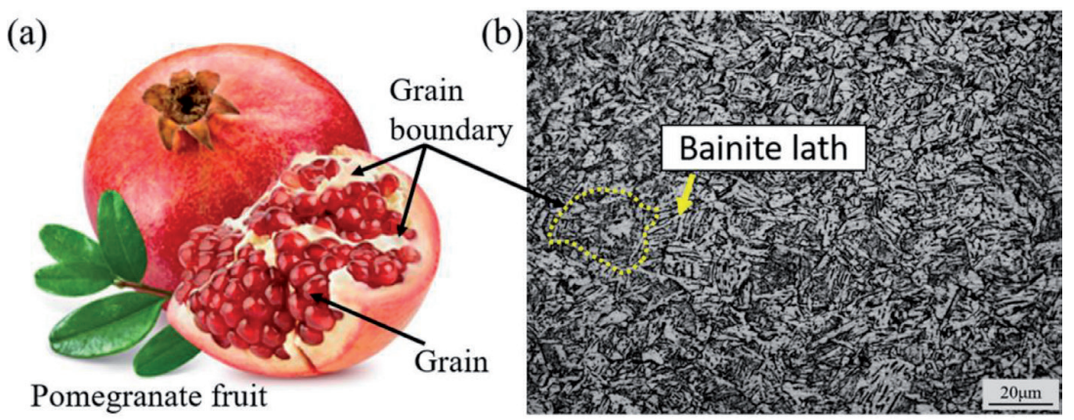

Figure 3.
The photographs of (a) pomegranate fruit, which compound of grains and separated by grain boundary like metal structure, (b) high strength steel structure consists of bainitic ferrite and martensite [27].

4. Some basics of plastic deformation mechanism

We know that the plastic deformation permanently changes the dimension and shape of metal, whereas in terms of microstructural changes only the number density of dislocations increases, whereas crystal structures including lattice parameters of metals typically remain unchanged. Slip and twinning processes, which are shown in a simple model presentation in **Figure 4**, are responsible for this macroscopic change of shape and dimensions. Slip implicates sliding of abutting blocks of a crystal along definite crystallographic planes, called slip planes. A slip occurs when shear stress applied to the material exceeds a critical value. During slip, each atom usually moves the same integral number of atomic distances along the slip plane producing a step, without change of the crystal orientation (**Figure 4b**). Grain boundaries represent obstacles for the slip movement as the slip direction, according to **Figure 4a**, will be usually changed across the boundary. This implies

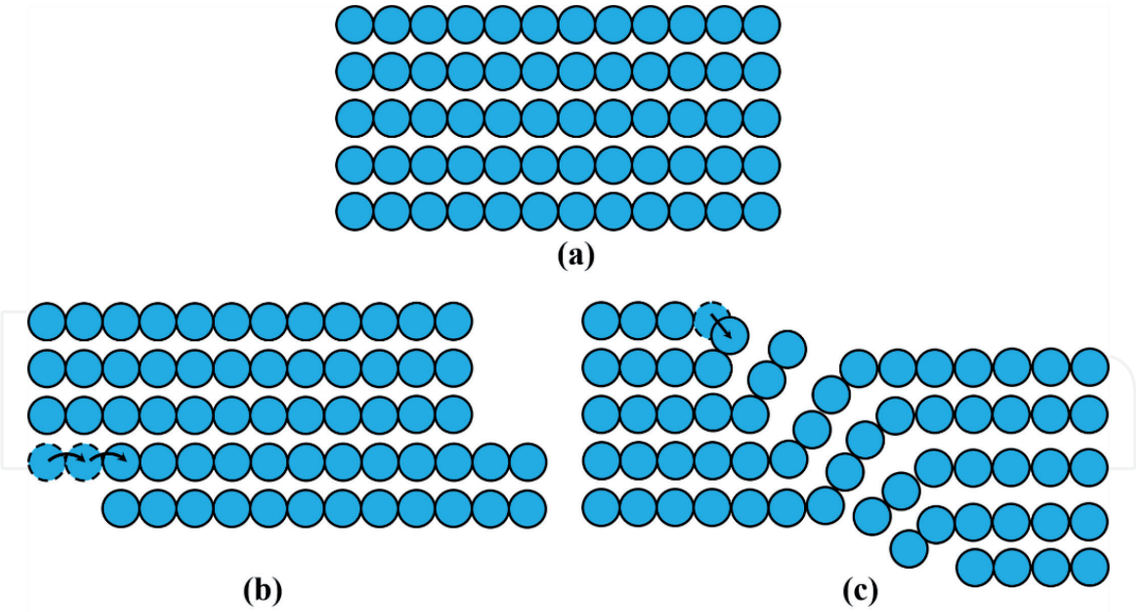

Figure 4.
Schematic representation of slip and twinning mechanisms in metals during plastic deformation (a) original position of atoms within a crystal lattice, (b) atoms movement by slip, (c) atoms movement by twinning [43].

that the strength of polycrystalline materials will be higher than that of a single crystal of the same material.

In twinning, each atom moves by only a fraction of an interatomic distance relative to its neighboring atoms (see **Figure 4c**). The twinned portion of the crystal is a mirror image of the parent crystal. The orientation of the twinned region is however different from the untwinned region (**Figure 4a**).

5. Terminology and summary of TMP related mechanisms

Metallurgical incidents during the TMP may act statically or dynamically on the material. This depends upon the rate of load and temperature conditions and strongly affects grain refinement. Microstructural evolution during TMP largely depends on the ability of dislocation movement during plastic deformation, which has consequently also a considerable impact on the mechanical properties of materials. The terminology of several mechanisms related to TMP is introduced in the following. These can be understood with the help of the flow stress–strain diagram (**Figure 5**) interpretation [44]. The flow stresses σ_c, σ_p, and σ_s mean the critical, peak, and steady state conditions, respectively. The combined effect of work hardening (WH) and softening mechanisms on flow curves are categorized into distinct regions: I) hardening, II) critical, III) softening and IV) steady-state. WH and dynamic recovery (DRV) occur in the first region where WH dominates and flow stress rises steeply. The second region is the critical zone where DRV and WH both are decreased and new dynamic recrystallization (DRX) initiates. Subsequently, DRX is clearly observed in the third region associated with softening. The fourth region is a steady-state where only DRX occurs. Key mechanisms and their terminology are treated in detail in the following.

5.1 Work hardening

Work hardening (WH) is also called strain hardening or cold hardening. It is the process of making a metal stronger and harder below its recrystallization

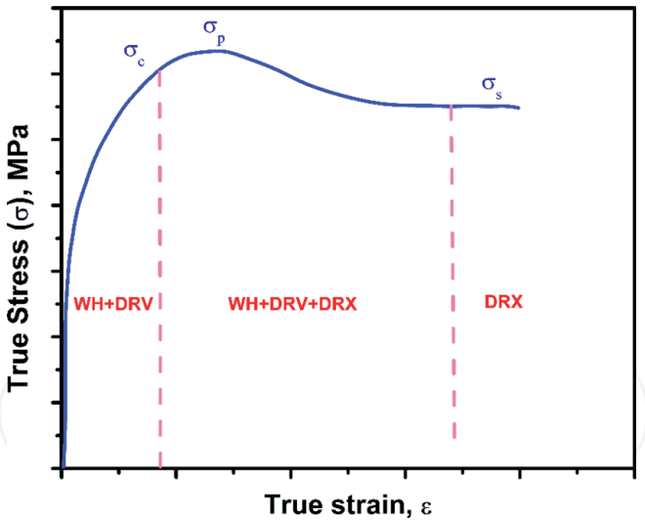

Figure 5.
Schematic flow stress–strain diagram [44].

temperature by increasing dislocation density via plastic deformation. Dislocations will be pinned by each other. Also, as a consequence this highly "faulted" microstructure will prevent the propagation of cracks. With increasing the temperature, the chance of rearrangement of matter and also dislocations is higher which contributes to lower strength at increased ductility.

5.2 Recovery

Recovery is a softening process that refers to the relieve of part of the internal energy stored within the microstructure, taking place before recrystallization in a deformed material. It normally occurs above the recrystallization temperature where the movement of atoms, i.e. the atomic mobilities and derived diffusion is considerably facilitated. Diffusion increases rapidly with rising temperatures and tends to recover strained regions to the "original" unstrained structure (**Figure 6a**). The extent of recovery depends, among other parameters, on the stacking fault energy (SFE), the type and amount of solute atoms of the material, particularly in the context of dislocation dissociations, which determine the rate of dislocation climb and cross slip. In low SFE metals, recovery as well as cross slip and climb of dislocation is difficult, while the climb is rapid and significant recovery may occur in metals and alloys with a high SFE [46].

Two types of recovery are known, static and dynamic recovery. Static recovery (SRV) occurs at high strain rates where jerky microstructural response of dislocation dynamics prevails. Technologically, this is the case for instance during friction stir welding (FSW) and other torsion processing. Dynamic recovery (DRV) occurs at slower strain rates where thermal activation of the metastable positions within the dislocation structure leads to steady-state during metal processing e.g. hot-rolling, extrusion, and forging processes, It is commonly accepted that both DRV and SRV reduce the stresses through changes in dislocation structure due to subgrain growth, dislocation annihilation, and dislocation rearrangement into lower-energy configurations (such as planar dislocation boundaries). Overall, ductility is improved by recovery, while the strength of materials is reduced [47].

5.3 Recrystallization

The recrystallization associates with the nucleation of new strain-free grains and their subsequent growth in deformed microstructure when internal energy reaches a critical value (**Figure 6b** and **c**). When the recrystallization process arises during

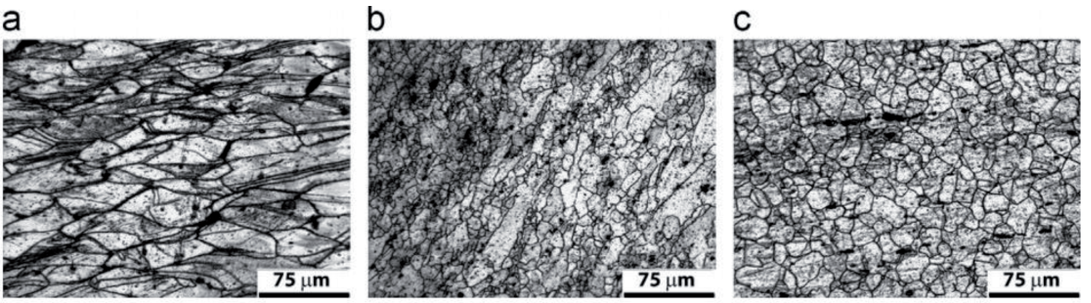

Figure 6.
The optical microstructure of deformed stainless steel samples: (a) recovered grains (b) partial recrystallization (c) area of full recrystallization [45].

Type of process	Mechanism	Materials type
Hot deformation ($T > 0.5T_m$)	dDRX	Category L & M
	cDRX and DRV	Category H
Cold/warm deformation ($T < 0.5T_m$)	cDRX	All Categories
Hot torsion ($T > 0.5T_m$), other SPD processes	DRV + dDRX+cDRX	All Categories

Where,
Low and medium-range SFE materials (*Category L & M*): Copper, Gold, Lead, γ-iron, Ni and their alloys.
High SFE materials (*Category H*): Aluminum, Magnesium, α-iron, and their alloys.

Table 2.
The details of materials and acting mechanisms during the hot deformation process [34, 49, 50].

deformation processes, it is called dynamic recrystallization (DRX). In contrast, when it takes place after deformation or during post-processing like the annealing process, it is known as static recrystallization (SRX) [48]. When DRX is not completed within deformation, this is termed meta dynamic or post dynamic DRX (mDRX) [48]. Moreover, two types of DRX can be distinguished. In discontinuous DRX (dDRX) strain-free grains nucleate and grow rapidly, thus consuming the surrounding strain hardened matrix, while continuous DRX (cDRX) involves the generation of new grain boundaries by the continuous misorientation of nearby subgrains. The combined effect of cDRX and dDRX phenomena takes place during higher strain conditions which are possible during torsion, other severe plastic deformation processes [29]. Since the rate of annihilation due to dynamic recovery is not sufficient to complete with the strain hardening rate in low SFE materials, the dislocation density increases continuously in this case. Contrary, high SFE materials act in favor for higher mobility of dislocation, and consequently dynamic recovery becomes involved as an operating mechanism [49]. The details of materials and the type of possible phenomena are illustrated in **Table 2**.

The range of dDRX and cDRX can be understood through the schematic diagram between processing temperature and strain rate (see **Figure 7a**). dDRX phenomena increase above the melting temperature (T_m) when the strain rate decreases while the cDRX phenomena decrease with decreases in processing temperature and increases in strain rate. cDRX occurs in all SFE materials [53] when the temperature falls below 0.5 T_m, however, the dDRX takes place only in low and medium-range SFE materials above 0.5 T_m wherein dynamic recovery is slow after accessing a critical strain value, as can be seen in **Figure 7a** [34, 54, 55]. The grain nucleation and growth during dDRX is the same as for primary DRX which occurs during heating in cold-worked materials. Localized nucleation and growth at local grain boundary

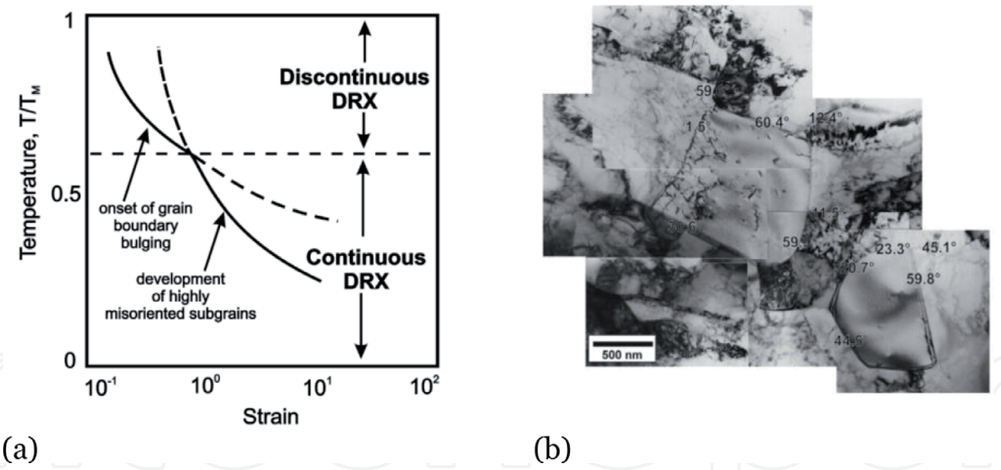

Figure 7.
(a) Schematic correlation between cDRX and dDRX [51], (b) dDRX nuclei in austenitic stainless steel at 800°C with strain rate 0.001 s^{-1} [52].

bulging can be seen in **Figure 7b**. It is obvious that the dDRX nuclei contain a much lower dislocation density than the deformed region and these nuclei are distinct from highly disturbed substructures with twin boundaries and low angle dislocation sub boundaries.

One additional terminology has recently been denoted as post-DRX which occurs during the annealing process in deformed materials [55].

6. Impact of plastic deformation parameters on microstructure and properties evolution

Some major metal processing parameters such as temperature, strain rate, and strains that impact steel microstructures and their flow curves are illuminated in detail in the following.

6.1 The role of work-hardening rate

The WH rate enables strengthening and hardening to the materials below the recrystallization temperature. Rapid WH rates are realized in low strain regions due to increases in dislocation density while at later strain increase, the effect starts to decrease due to recrystallization of new strain-free grains [31, 36, 40, 50, 56]. In WH, dislocations are preferably pinned, which will impede crack propagation on the microscale. With increasing temperature, the probability of rearrangement of atoms is higher which assists lower strength but increases the ductility of materials. Samantaray et al. [36] have reported for 316 L stainless steel that the WH rate starts rapidly with increasing temperature and strain rate at a specific value of strain (see **Figure 8**). The WH rate gradually decreased at higher temperature with increasing strain while it falls more rapidly under lower temperature conditions.

Lin et al. [44] have derived the following model for the influence of dynamic recovery during WH (see Eq. (2)) and dynamic recrystallization Eq. (3) under different deformation conditions within TMP.

$$\sigma = [\sigma_{DRV}^2 + (\sigma_0^2 - \sigma_{DRV}^2)\exp(-\Omega\,\varepsilon)]^{0.5} \tag{2}$$

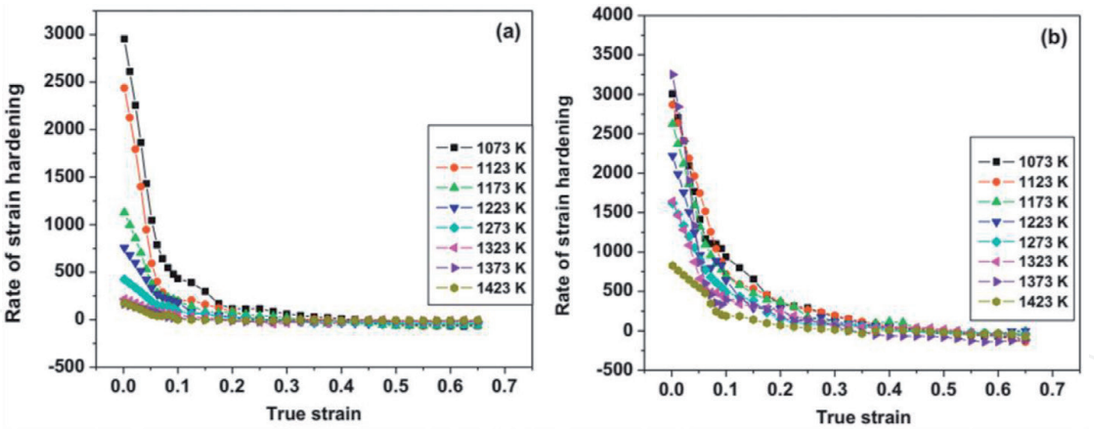

Figure 8.
The impact of temperature and strain rate on work hardening rate of stainless steel [57].

$$\sigma = \sigma_{DRV} - \left(\sigma_P - \sigma_{DRX}\right)\left\{1 - exp\left[-K_d\left(\frac{\varepsilon - \varepsilon_c}{\varepsilon_P}\right)^{n_d}\right]\right\} \varepsilon \geq \varepsilon_c \tag{3}$$

Where σ is flow stress; σ_{DRV} is steady-state stress due to dynamic recovery; σ_{DRV} is steady-state stress due to dynamic recrystallization; σ_0 is yield stress; ε is strain; ε_P is peak strain; ε_c is critical strain; Ω is coefficient of dynamic recovery.

Generally, the critical strain acknowledgeable for the start of DRX can be calculated either by deformed microstructure or flow stress curves [58], In which flow stress curve analysis are simple and easier while microstructural are complicated. This flow curve analysis method was proposed in 1981 by Mecking et al. [59] and later it developed by Ryan et al. [60] and McQueen et al. [61] emphasize the point where DRX occurs on the flow curves. This method allows to find out the critical strain point where the flow curve changes due to the formation of new strain-free grains via DRX.

6.2 On properties derived from flow curves and relation to microstructures

The flow stress–strain curve reflects the changes in the material through plastic deformation during dynamic loading [25, 32, 62–66]. The flow stress can be influenced by several factors like chemical composition, crystal structure (e.g., steel matrix - bcc, fcc, Mg-base - hcp, and others) [50, 67], different phases and compounds [17, 30, 50, 68–70], grain boundaries [25, 50, 71, 72] as well as imperfections [34, 50, 55, 73, 74]. Other factors such as friction (σf), thermal (σt) and athermal (σa) terms also affect flow stresses, as indicative by relations in Eq. (4) [75].

$$\sigma = \sigma_f\left(\dot{\varepsilon}, T\right) + \sigma_t\left(\dot{\varepsilon}, \varepsilon, T\right) + \sigma_a \tag{4}$$

Where T is temperature, $\dot{\varepsilon}$ is strain rate and ε is strain. σ_a represents the internal stress which occurs due to long range barriers to dislocation motion in the materials, while σ_f term reflects the stress needed to overcome the lattice friction depending on strain rate and temperature.

In addition, processing temperatures and strain rates are equally important for the plastic deformation behavior. Therefore, the dynamics of TMP can be understood through the investigation of microstructural changes combined with interpretations of trends of flow stress–strain curves which depend on DRV and DRX, and SRX [76, 77]. I.

It is noticed in most cases that flow stress decreases with increase in temperature and depends upon the applied strain rate [27, 32, 36, 78]. In terms of temperature, strain, and strain rates, the flow curves can be expressed by Eq. (5) [75].

$$\sigma = \frac{2}{\sqrt{3(1-m)}} K\varepsilon^{n}\, \dot{\varepsilon},^{m} \exp(-\beta T) \tag{5}$$

Where m stands for strain rate sensitivity, n represents the strain hardening exponent, and K, β represents material constant.

In the following, some flow curve trends of different steels and underlying phenomena are discussed.

Researchers reported that the series of flow curves are subjected to different temperatures and strain rates for different grades of steels [26, 27, 44, 45, 64]. Lin et al. [44] have reported interesting results for hot deformation of 42CrMo grade high strength steel in which they found that flow stress increased with decreasing temperature (**Figure 9a**) while it increased with strain rates (**Figure 9b**). At the slower strain rate in different ranges of temperatures, the flow stress will decrease with increase in temperature due to increase in the amount of cross slip screw dislocations and climb of edge dislocations, as well as vacancy diffusion. This results in an increase of grain boundary mobility and energy accumulation at boundaries for the nucleation and growth in DRX grains and dislocation annihilation which is responsible for the decrease in flow stress [27, 64].

Kumar et al. [27] have found for hot deformed condition in high strength steel that flow stress increases continuously at lower deformation temperature (750–850°C) due to continuation of work hardening phenomena High temperature showed the higher steady-state condition where DRX was dominant. While both DRV and DRX were dominant at all strain rates with decreasing temperature, the dDRX phenomena was more prominent at slow strain rate (0.001 s-1) at 900°C due to nucleation of unstrained grains that occurs normally in low SFE high strength steels. A flow curve without pronounced peak stress, but which exhibits

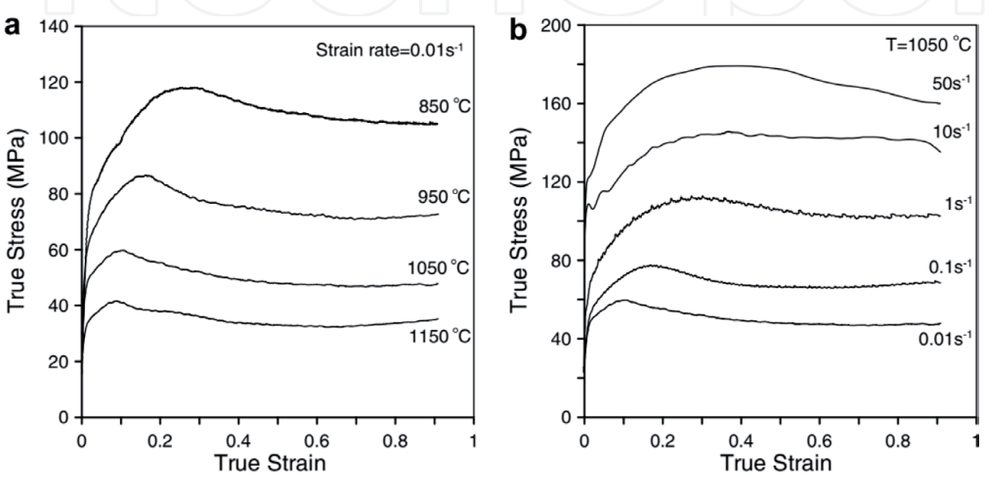

Figure 9.
The true stress–strain curves at different temperatures and strain rates for 42CrMo steel [44].

a steady-state, is generally associated with dynamic recovery being the dominant restoration mechanism [79].

Zhang et al. [31] have reported that several original grains were broken and recrystallized new grains showed up along the grain boundaries at the deformed condition at 900°C with a high strain rate 10 s^{-1}, which indicates that the deformed morphology is inhomogeneous. In contrast, at the same temperature but with a lower strain rate (1 s^{-1}), DRX was observed along the grain boundaries. This is due to local temperature rise within the samples during deformation. It is interesting to note that at the initial stage of strain, the flow stress increases steeply due to work hardening phenomena in materials having higher carbon content and less austenite stabilizing alloying elements. It reaches a peak value before going into the softening stage.

Souza et al. [45] have documented results of hot deformation testing at elevated temperatures with different strain rates in austenitic stainless steel. Also, some differences could be seen in the work hardening phenomena; the slopes of the flow stress curves changed. In the initial work hardening region, the increase of dislocation density during deformation is controlled by the competition between storage and annihilation of dislocations, i.e. opposing contributions of work hardening and the dynamic recovery due to the change of dislocation density with deformation.

7. SPD impacts on the structure and mechanical properties of steels

Severe plastic deformation where metal grains are heavily deformed is realized by using several setups of plastic deformations like high-pressure torsion, equal channel angle pressing, multi-axial forging, twist extrusion, accumulated roll bending, and constrained groove pressing [22, 34, 80]. Severe deformation produces not only a strong direct impact on the mechanical properties i.e. high strength, low-temperature toughness, superior plasticity, good ductility, and good wear resistance of high manganese grades steel but also on other important properties such as thermal stability, diffusion, radiation tolerance, and corrosion properties, which are indirectly associated with material stability and durability.

The high manganese steels (Mn) are advanced high strength austenitic steels that contain Mn between 3 to 31% wt. These steels are known as Hadfield steel, damping steel, complex steel, transformation induced plasticity steel (TRIP), and twinning induced plasticity steel (TWIP) [81, 82]. In all of these, Hadfield steel was firstly discovered in 1882 by Sir Robert Hadfield [83] while TWIP steel is one of the latest fully austenitic steel which is developed in the early 1990s by Japanese steelmakers Kobo steel, Nippon, and Sumitomo steel organizations.

It is well known that ultrafine and nanocrystalline structure depends on three mechanisms; martensitic transformation, dislocation motion, and twinning and twin evolution where stacking fault energy (SFE) of material plays an important role. **Figure 10** reflects the relation between strain-induced mechanism vs. temperature and SFE for Fe-20Mn-4Cr-0.5C steel. It shows that retained austenite can be converted into ε-martensite and strain-induced by a twinning mechanism at a lower temperature. Thus, the calculation of martensitic start temperature *and* SFE value is necessary to achieve the right combination of mechanical and other properties in low SFE high Mn steels. It is well known that the SFE of materials depends on chemical composition and on temperature [84–86]. The high Mn steels have a low SFE between 15 to 50 mJ/m2 [31, 85, 87].

Allain et al. [86] reported results for Fe-22Mn-0.06C steel where the temperature influences the SFE values and strain-induced mechanism, which can be seen in **Table 3**. The strain hardening and mechanical behavior of steels strongly depend

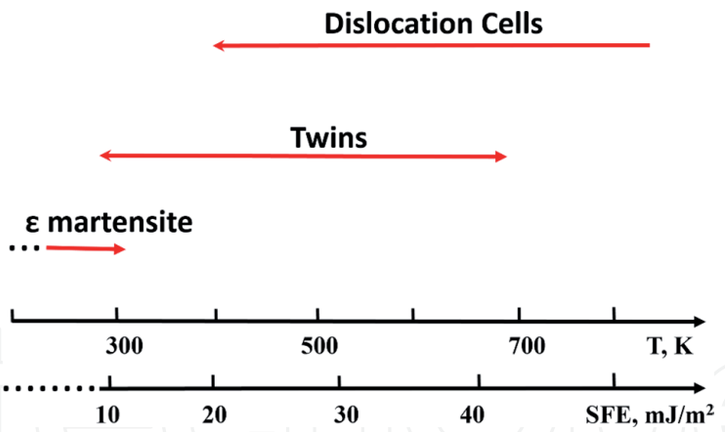

Figure 10.
Effect of SFE and temperature on deformation mechanism in Fe-20Mn-4Cr-0.5C steel [84].

Temperature, K	SFE value, mJ/m^2	Plasticity mechanism
77	10	Dislocation gliding
293	19	Dislocation gliding and twinning
673	80	Dislocation gliding and ε-martensitic transformation.

Table 3.
The deformation mechanism at different temperatures for Fe-22Mn-0.6C steel [86].

on the SFE, which is responsible for the activation energy of a deformation mechanism [87].

The mechanical properties of Hadfield Mn austenitic steels can be improved through high rate strain hardening where two phenomena (i.e. dislocation accumulation and twinning) act preferentially during plastic deformation [82]. This is attributed to the strain hardening transformation where austenite phase transforms into ε or α-martersite, and twinning, dynamic strain aging, dispute between dislocations with stacking faults occurs. In this connection, Yan et al. [88] have tried to improve the hardness values by shot pinning method, whereby hardness values could be increased with increasing in operation time. This was attributed to the increment in density of dislocations, dislocation accumulation, and formation of twinning. The influence of higher strain rate (between 10^3 to 10^5/s) attains great impact on mechanical behavior and wear resistance properties of high austenitic Mn steel which may be linked to dynamic strain aging and may delay fracture [81, 89–93].

Over the past few years, many researchers have reported work on TRIP and TWIP steels and achieved better mechanical properties by plastic deformation at high strains (more than 1) [22, 73, 74, 81, 89, 91, 94–96]. Both TRIP and TWIP steels are fully austenitic steels with less carbon content than hadfield steel. The initial microstructure of TRIP steel is consisted of martensite, bainite and ferrite with retained austenite. The fraction of carbon enriched retained austenite in TRIP steels is between 5 to 30% which transforms into martensite by displacive mechanism during SPD process. This behavior has attained great improvement in strength and toughness properties [96, 97].

A critical issue remains hydrogen embrittlement in TRIP steels, promoted by a displacive mechanism where the relevance of different solubility and diffusivity in the parent austenite has been discussed [96].

Sevsek et al. [90] reported the effect of strain rate on medium Mn X6MnAl12–3 steel. The softer austenite region was strained locally and transformed into

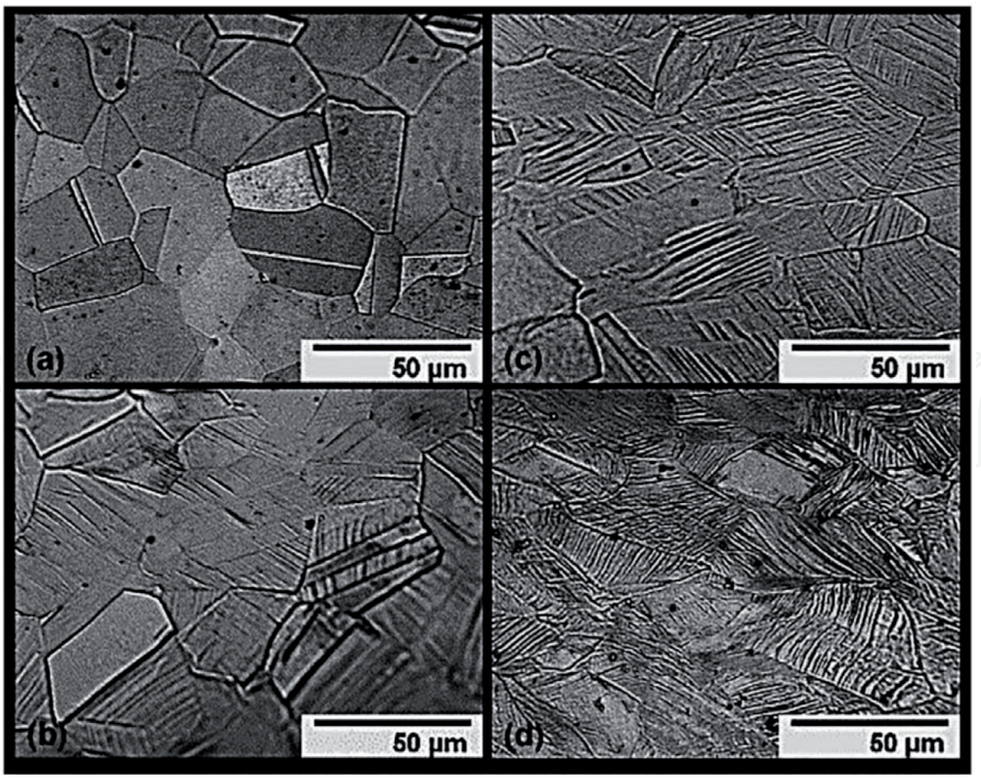

Figure 11.
Optical morphologies of Fe-22Mn-0.6C steel subjected to high strain deformation: (a) unstained; strained with (b) 18%, (c) 26%, and (d) 34% [81].

martensite which depended on the strain rate sensibility. The deformation induced phase transformation of austenite to martensite is partially suppressed at lower and higher strain rates. The impact of high strains in fully austenitic Fe-22Mn-0.6C steel is predominantly controlled by twinning plasticity mechanism (see **Figure 11**) as suggested by Jacob et al. [81]. The initial microstructure of Fe-22Mn-0.6C steel is a single-phase austenitic steel with few twinned grains (**Figure 11a**). They found that the fraction of twinning is increased with increasing strains (**Figure 11b–d**), where most of the internal energy was used for recrystallization and rest for grain growth [87]. They concluded that twin boundaries act as a hindrance to the dislocation glide providing work hardening effect.

In the same way, Kang et al. [98] have reported HPT tests for TWIP steel, in which they found that both stress and hardness values increased with an increase in the number of turns. This was related to grain refinement. It was also noticed that the inhomogeneity in morphology and volume of low and high angle grain boundaries increased with the increase in the number of turns, associated with higher stress and lower elongation. The hardness at tip location was found to be lower in all strain ranges due to the lower extent of plastic deformation while at the edge it was higher.

8. Concluding remarks

This review chapter focuses on plastic deformation behavior which can be controlled via processing parameters. Their optimisation is responsible for a refined microstructure, typically associated with beneficial mechanical properties of metals and steel due to metal forming. In other words, an appropriate combination of processing parameters enables one to fabricate products that will be defect-free on

the microscale, which represents an important demand of customers. It is noticed that the flow stress increases with an increase in strain rate when the temperature is constant while it decreases with an increase in temperature when the strain rate is constant. The dDRX phenomena occur under axial stress hot deformation conditions while cDRX phenomena are linked to torsion deformation conditions during severe plastic deformation at relatively low temperatures. Plastic deformation acts differently in the case of high Mn austenitic TRIP steels where retained austenite is transformed into martensite by displacive mechanism and induced strain forms twinning which improves strength and toughness of steels. In contrast, the high-Mn fully austenitic steel such as TWIP steels generate huge amount of twinning structure by induced high strains and do not show phase transformation like TRIP steels.

Author details

Sanjeev Kumar[1*] and Erwin Povoden-Karadeniz[1,2]

1 Christian Doppler Laboratory for Interfaces and Precipitation Engineering CDL-IPE, Technische Universität Wien, Vienna, Austria

2 Institute of Materials Science and Technology, Technische Universität Wien, Vienna, Austria

*Address all correspondence to: sanjeev.kumar@tuwien.ac.at

References

[1] R. A. Anderson, M. W. Touma, G. Ashe, and J. F. Conlon, "Optimized Design Parameters for Welded Tmcp Steels," 1997.

[2] A. Forgas Júnior, J. Otubo, and R. Magnabosco, "Ferrite quantification methodologies for duplex stainless steel," J. Aerosp. Technol. Manag., vol. 8, no. 3, pp. 357-362, 2016, doi:10.5028/jatm.v8i3.653.

[3] A. Chatterjee, A. Moitra, A. K. Bhaduri, D. Chakrabarti, and R. Mitra, "Effect of heat treatment on ductile-brittle transition behaviour of 9Cr-1Mo steel," *Procedia Eng.*, vol. 86, no. July 2016, pp. 287-294, 2014, doi: 10.1016/j.proeng.2014.11.040.

[4] O. G. Comineli, "Investigations on the Influence of Oxidation in Causing Hot Cracking in Steels," in *Thermo-mechanical Simulation and Processing of Steels (SimPro '16), Ranchi, India*, 2016, no. Feb, pp. 579-588.

[5] Q. Xue, D. Benson, M. a. Meyers, V. F. Nesterenko, and E. a. Olevsky, "Constitutive response of welded HSLA 100 steel," Mater. Sci. Eng. A, vol. 354, no. 1-2, pp. 166-179, 2003, doi: 10.1016/S0921-5093(03)00007-8.

[6] S. Kumar, S. K. Nath, and V. Kumar, "Continuous cooling transformation behavior in the weld coarse grained heat affected zone and mechanical properties of Nb-microalloyed and HY85 steels," Mater. Des., vol. 90, pp. 177-184, 2016, doi: 10.1016/j.matdes.2015.10.071.

[7] T. Y. Hsu and X. Jin, *Advanced Steels*. 2011.

[8] K. Jármai and B. Bolló, *Vehicle and Automotive Engineering*. 2017.

[9] D. Niu, J. Zhang, P. Xiong, G. Hao, S. Liu, and W. Guo, "High temperature fatigue and oxidation characteristics of forged steel piston materials," *Eng. Fail. Anal.*, vol. 97, no. January, pp. 220-226, 2019, doi: 10.1016/j.engfailanal.2019.01.014.

[10] R. Feng, S. Li, Z. Li, and L. Tian, "Variations of microstructure and properties of 690MPa grade low carbon bainitic steel after tempering," Mater. Sci. Eng. A, vol. 558, pp. 205-210, 2012, doi: 10.1016/j.msea.2012.07.113.

[11] B. Basu, S. M. Tripathi, and V. V. Modak, "Thermomechanically-controlled processing for producing ship-building steels," Def. Sci. J., vol. 55, no. 1, pp. 91-101, 2005.

[12] E. J. Czyryca, "Development of Low-Carbon , Copper-Strengthened HSLA Steel Plate for Naval Ship Construction."

[13] A. Sharma, A. Kumar, and R. Tyagi, "Erosive wear analysis of medium carbon dual phase steel under dry ambient condition," *Wear*, vol. 334-335, no. July 2015, pp. 91-98, 2015, doi: 10.1016/j.wear.2014.12.005.

[14] S. Kumar, "Isothermal Transformation Behavior and Microstructural Evolution of Micro-Alloyed Steel," in *Engineering Steels and High Entropy-Alloys*, A. Sharma, S. Kumar, and Z. Duriagina, Eds. IntechOpen Publication Dondon, 2020, pp. 27-36.

[15] L. Ma, J. Han, J. Shen, and S. Hu, "Effects of Microalloying and Heat-Treatment Temperature on the Toughness of 26Cr–3.5Mo Super Ferritic Stainless Steels," Acta Metall. Sin. (English Lett., vol. 27, no. 3, pp. 407-415, 2014, doi: 10.1007/s40195-014-0070-2.

[16] J. Dille *et al.*, "Influence of Heat Treatments on Microstructure and Magnetic Domains in Duplex Stainless

Steel S31803," Metall. Mater. Trans. A Phys. Metall. Mater. Sci., vol. 49, no. 8, pp. 3515-3524, 2018, doi: 10.1007/s11661-018-4721-1.

[17] A. Lambert-Perlade, A. F. Gourgues, and A. Pineau, "Austenite to bainite phase transformation in the heat-affected zone of a high strength low alloy steel," Acta Materialia, vol. 52, no. 8. pp. 2337-2348, 2004, doi: 10.1016/j.actamat.2004.01.025.

[18] A. F. M. Pérez, M. Breda, I. Calliari, G. Y. P. Medina, and R. Sandström, "Detrimental Cr-rich phases precipitation on SAF 2205 duplex stainless steels welds after heat treatment," Soldag. Inspeção, vol. 21, no. 2, pp. 165-171, 2016, doi: 10.1590/0104-9224/SI2102.06.

[19] Y. Mouadji, M. A. Bradai, R. Younes, A. Sad-eddine, and A. Benabbas, "Influence of heat treatment on microstructure and tribological properties of flame spraying Fe-Ni-Al alloy coating," J. Cent. South Univ., vol. 25, no. 3, pp. 473-481, 2018, doi: 10.1007/s11771-018-3751-6.

[20] S. Kumar and S. K. Nath, "Effect of weld thermal cycles on microstructures and mechanical properties in simulated heat affected zone of a HY 85 steel," Trans. Indian Inst. Met., pp. 1-12, 2016, doi: 10.1007/s12666-016-0880-1.

[21] V. Segal, "Review: Modes and processes of severe plastic deformation (SPD)," *Materials (Basel).*, vol. 11, no. 7, 2018, doi: 10.3390/ma11071175.

[22] Y. Estrin and A. Vinogradov, "Extreme grain refinement by severe plastic deformation: A wealth of challenging science," Acta Mater., vol. 61, no. 3, pp. 782-817, 2013, doi: 10.1016/j.actamat.2012.10.038.

[23] S. Kim, Y. Kang, and C. Lee, "Effect of thermal and thermo-mechanical cycling on the boron segregation behavior in the coarse-grained heat-affected zone of low-alloy steel," Mater. Charact., vol. 116, pp. 65-75, 2016, doi: 10.1016/j.matchar.2016.04.004.

[24] F. Njock Bayock, P. Kah, P. Layus, and V. Karkhin, "Numerical and Experimental Investigation of the Heat Input Effect on the Mechanical Properties and Microstructure of Dissimilar Weld Joints of 690-MPa QT and TMCP Steel," *Metals (Basel).*, vol. 9, no. 3, p. 355, 2019, doi: 10.3390/met9030355.

[25] S. K. Rajput, G. P. Chaudhari, and S. K. Nath, "Characterization of hot deformation behavior of a low carbon steel using processing maps, constitutive equations and Zener-Hollomon parameter," J. Mater. Process. Technol., vol. 237, pp. 113-125, 2016, doi: 10.1016/j.jmatprotec.2016.06.008.

[26] N. Kumar, S. Kumar, S. K. Rajput, and S. K. Nath, "Modelling of Flow Stress and Prediction of Workability by Processing Map for Hot Compression of 43CrNi Steel," ISIJ Int., vol. 57, no. 3, pp. 497-505, 2017, doi: 10.2355/isijinternational.ISIJINT-2016-306.

[27] S. Kumar, S. K. Rajput, N. Kumar, and N. S. K., "Understanding Hot Workability and Flow Stress Prediction through Processing Map with Microstructural Correlation for HY85 Steel," Mater. Perform. Charact., vol. 9, no. 12, pp. 134-149, 2019.

[28] G. E. Dieter, *Mechanical Metallurgy*, Third edit. McGraw-Hill, New York, 1988.

[29] E. Bagherpour, N. Pardis, M. Reihanian, and R. Ebrahimi, "An overview on severe plastic deformation: research status, techniques classification, microstructure evolution, and applications," Int. J. Adv. Manuf. Technol., vol. 100, no. 5-8, pp.

1647-1694, 2019, doi: 10.1007/s00170-018-2652-z.

[30] K. Edalati, "Review on Recent Advancements in Severe Plastic Deformation of Oxides by High-Pressure Torsion (HPT)," Adv. Eng. Mater., vol. 21, no. 1, pp. 1-10, 2019, doi: 10.1002/adem.201800272.

[31] J. Zhang, H. Di, K. Mao, X. Wang, Z. Han, and T. Ma, "Processing maps for hot deformation of a high-Mn TWIP steel: A comparative study of various criteria based on dynamic materials model," Mater. Sci. Eng. A, vol. 587, pp. 110-122, 2013, doi: 10.1016/j.msea.2013.08.036.

[32] S. K. Rajput, G. P. Chaudhari, and S. K. Nath, "Physical Simulation of Hot Deformation of Low-Carbon Ti-Nb Microalloyed Steel and Microstructural Studies," J. Mater. Eng. Perform., vol. 23, no. 8, pp. 2930-2943, 2014, doi: 10.1007/s11665-014-1059-8.

[33] G. Faraji and H. S. Kim, "Review of principles and methods of severe plastic deformation for producing ultrafine-grained tubes," Mater. Sci. Technol. (United Kingdom), vol. 33, no. 8, pp. 905-923, 2017, doi: 10.1080/02670836.2016.1215064.

[34] T. Sakai, A. Belyakov, R. Kaibyshev, H. Miura, and J. J. Jonas, "Dynamic and post-dynamic recrystallization under hot, cold and severe plastic deformation conditions," Prog. Mater. Sci., vol. 60, no. 1, pp. 130-207, 2014, doi: 10.1016/j.pmatsci.2013.09.002.

[35] C. C. F. Kwan and Z. Wang, "The cyclic deformation behavior of severe plastic deformation (SPD) metals and the influential factors," Metals (Basel)., vol. 2, no. 1, pp. 41-55, 2012, doi: 10.3390/met2010041.

[36] D. Samantaray, S. Mandal, C. Phaniraj, and A. K. Bhaduri, "Flow behavior and microstructural evolution during hot deformation of AISI Type 316 L(N) austenitic stainless steel," Mater. Sci. Eng. A, vol. 528, no. 29-30, pp. 8565-8572, 2011, doi: 10.1016/j.msea.2011.08.012.

[37] N. Kumar, S. Kumar, S. K. Rajput, and S. K. Nath, "Modelling of flow stress and prediction of workability by processing map for hot compression of 43CrNi steel," *ISIJ Int.*, vol. 57, no. 3, 2016.

[38] D. Samantaray, A. Chaudhuri, U. Borah, A. K. Bhaduri, and P. Dutta, "Role of grain boundary ferrite layer in dynamic recrystallization of semi-solid processed type 304L austenitic stainless steel," Mater. Lett., vol. 179, pp. 65-68, 2016, doi: 10.1016/j.matlet.2016.05.049.

[39] Z. Yang, F. Zhang, C. Zheng, M. Zhang, B. Lv, and L. Qu, "Study on hot deformation behaviour and processing maps of low carbon bainitic steel," Mater. Des., vol. 66, pp. 258-266, 2015, doi: 10.1016/j.matdes.2014.10.068.

[40] Y. C. Lin, M. S. Chen, and J. Zhang, "Modeling of flow stress of 42CrMo steel under hot compression," Mater. Sci. Eng. A, vol. 499, no. 1-2, pp. 88-92, 2009, doi: 10.1016/j.msea.2007.11.119.

[41] M. Furukawa, Z. Horita, and T. Langdon, *Severe plastic deformation*. 2004.

[42] S. Nemat-Nasser, "Introduction to High Strain Rate Testing," ASM Handb. Int., vol. 8, pp. 427-428, 2000.

[43] V. Raghavan, *Physical metallurgy*, vol. 2. 2012.

[44] Y. C. Lin, M. S. Chen, and J. Zhong, "Prediction of 42CrMo steel flow stress at high temperature and strain rate," Mech. Res. Commun., vol. 35, no. 3, pp. 142-150, 2008, doi: 10.1016/j.mechrescom.2007.10.002.

[45] R. C. Souza, E. S. Silva, A. M. Jorge, J. M. Cabrera, and O. Balancin, "Dynamic recovery and dynamic recrystallization competition on a Nb- and N-bearing austenitic stainless steel biomaterial: Influence of strain rate and temperature," Mater. Sci. Eng. A, vol. 582, pp. 96-107, 2013, doi: 10.1016/j.msea.2013.06.037.

[46] E. J. Giordani, A. M. Jorge, and O. Balancin, "Proportion of recovery and recrystallization during interpass times at high temperatures on a Nb- and N-bearing austenitic stainless steel biomaterial," Scr. Mater., vol. 55, no. 8, pp. 743-746, 2006, doi: 10.1016/j.scriptamat.2006.05.015.

[47] A. Heidarzadeh *et al.*, "Friction stir welding/processing of metals and alloys: A comprehensive review on microstructural evolution," *Prog. Mater. Sci.*, no. October, p. 100752, 2020, doi: 10.1016/j.pmatsci.2020.100752.

[48] B. Mirzakhani, M. T. Salehi, S. Khoddam, S. H. Seyedein, and M. R. Aboutalebi, "Investigation of dynamic and static recrystallization behavior during thermomechanical processing in a API-X70 microalloyed steel," J. Mater. Eng. Perform., vol. 18, no. 8, pp. 1029-1034, 2009, doi: 10.1007/s11665-008-9338-x.

[49] F. Montheillet, J. Lépinoux, D. Weygand, and E. Rauch, "Dynamic and static recrystallization," Adv. Eng. Mater., vol. 3, no. 8, pp. 587-589, 2001, doi: 10.1002/1527-2648(200108)3:8<587::AID-ADEM587>3.0.CO;2-V.

[50] N. Hansen and C. Y. Barlow, *Plastic Deformation of Metals and Alloys*, Fifth Edit., vol. 1. Elsevier, 2014.

[51] N. Dudova, A. Belyakov, T. Sakai, and R. Kaibyshev, "Dynamic recrystallization mechanisms operating in a Ni-20%Cr alloy under hot-to-warm working," Acta Mater., vol. 58, no. 10, pp. 3624-3632, 2010, doi: 10.1016/j.actamat.2010.02.032.

[52] A. Belyakov, T. Sakai, H. Miura, and R. Kaibyshev, "Grain Refinement under Multiple Warm Deformation in 304 type Austenitic Stainless Steel," ISIJ Int., vol. 39, no. 6, pp. 592-599, 1999.

[53] M. C. Poletti, R. Buzolin, S. Kumar, P. Wang, and T. F. J. Simonet-Fotso, "Microstructure evolution of ti-5al-5v-5mo-3cr after hot deformation at large and moderate strains," *Mater. Sci. Forum*, vol. 941 MSF, pp. 1443-1449, 2018, doi: 10.4028/www.scientific.net/MSF.941.1443.

[54] P. R. Rios, F. Siciliano, H. R. Z. Sandim, R. L. Plaut, and A. F. Padilha, "Nucleation and growth during recrystallization," Mater. Res., vol. 8, no. 3, pp. 225-238, 2005, doi: 10.1590/S1516-14392005000300002.

[55] M. Tikhonova, R. Kaibyshev, and A. Belyakov, "Microstructure and Mechanical Properties of Austenitic Stainless Steels after Dynamic and Post-Dynamic Recrystallization Treatment," Adv. Eng. Mater., vol. 20, no. 7, pp. 1-27, 2018, doi: 10.1002/adem.201700960.

[56] B. Gong, X. W. Duan, J. S. Liu, and J. J. Liu, "A physically based constitutive model of As-forged 34CrNiMo6 steel and processing maps for hot working," *Vacuum*, vol. 155, no. April, pp. 345-357, 2018, doi: 10.1016/j.vacuum.2018.06.022.

[57] D. Samantaray, S. Mandal, V. Kumar, S. K. Albert, A. K. Bhaduri, and T. Jayakumar, "Optimization of processing parameters based on high temperature flow behavior and microstructural evolution of a nitrogen enhanced 316L(N) stainless steel," *Mater. Sci. Eng. A*, vol. 552, no. July 2016, pp. 236-244, 2012, doi: 10.1016/j.msea.2012.05.036.

[58] T. Xi, C. Yang, M. Babar Shahzad, and K. Yang, "Study of the processing

map and hot deformation behavior of a Cu-bearing 317LN austenitic stainless steel," Mater. Des., vol. 87, pp. 303-312, 2015, doi: 10.1016/j.matdes.2015.08.011.

[59] H. Mecking and U. F. Kocks, "Kinetics of flow and strain-hardening," *Acta Metall.*, vol. 29, no. 11, pp. 1865-1875, 1981, doi: https://doi.org/10.1016/0001-6160(81)90112-7.

[60] N. D. Ryan and H. J. McQueen, "Flow stress, dynamic restoration, strain hardening and ductility in hot working of 316 steel," *J. Mater. Process. Technol.*, vol. 21, no. 2, pp. 177-199, 1990, doi: https://doi.org/10.1016/0924-0136(90)90005-F.

[61] H. J. McQueen, S. Yue, N. D. Ryan, and E. Fry, "Hot working characteristics of steels in austenitic state," *J. Mater. Process. Technol.*, vol. 53, no. 1, pp. 293-310, 1995, doi: https://doi.org/10.1016/0924-0136(95)01987-P.

[62] P. Gao, M. Fu, M. Zhan, Z. Lei, and Y. Li, "Deformation behavior and microstructure evolution of titanium alloys with lamellar microstructure in hot working process: A review," J. Mater. Sci. Technol., vol. 39, pp. 56-73, 2020, doi: 10.1016/j.jmst.2019.07.052.

[63] S. Patra, V. Kumar, A. Haldar, and D. Chakrabarti, "Effect of hot-deformation on micro-texture in ultra-fine grained HSLA steel," vol. 703, no. January, pp. 439-442, 2012, doi: 10.4028/www.scientific.net/MSF.702-703.439.

[64] F. Ren, F. Chen, J. Chen, and X. Tang, "Hot deformation behavior and processing maps of AISI 420 martensitic stainless steel," J. Manuf. Process., vol. 31, pp. 640-649, 2018, doi: 10.1016/j.jmapro.2017.12.015.

[65] B. Srinivas, C. Srinivasu, B. Mahesh, and M. Aqheel, "A Review on Severe Plastic Deformation," *Int. J. Adv. Mater. Manuf. Charact.*, vol. 3, no. 1, pp. 291-295, 2013, doi: 10.11127/ijammc.2013.02.053.

[66] M. K. Mishra, A. G. Rao, R. Sarkar, B. P. Kashyap, and N. Prabhu, "Effect of Preaging Deformation on Aging Characteristics of 2507 Super Duplex Stainless Steel," J. Mater. Eng. Perform., vol. 25, no. 2, pp. 374-381, 2016, doi: 10.1007/s11665-015-1840-3.

[67] P. O. Malta, F. L. Dias, A. C. M. de Souza, and D. B. Santos, "Microstructure and texture evolution of duplex stainless steels with different molybdenum contents," *Mater. Charact.*, vol. 142, no. June, pp. 406-421, 2018, doi: 10.1016/j.matchar.2018.06.006.

[68] J. L. del Abra-Arzola *et al.*, "Study of the effect of sigma phase precipitation on the sliding wear and corrosion behaviour of duplex stainless steel AISI 2205," *Wear*, vol. 400-401, no. August 2017, pp. 43-51, 2018, doi: 10.1016/j.wear.2017.12.019.

[69] R. Mahnken, A. Schneidt, T. Antretter, U. Ehlenbröker, and M. Wolff, "Multi-scale modeling of bainitic phase transformation in multi-variant polycrystalline low alloy steels," Int. J. Solids Struct., vol. 54, pp. 156-171, 2015, doi: 10.1016/j.ijsolstr.2014.10.021.

[70] M. F. Ashby, "The deformation of plastically non-homogeneous materials," Philos. Mag., vol. 21, no. 170, pp. 399-424, 1970, doi: 10.1080/14786437008238426.

[71] H. J. McQueen, "Dynamic Recovery and Recrystallization," Encycl. Mater. Sci. Technol., pp. 2375-2381, 2001, doi: 10.1016/b0-08-043152-6/00419-8.

[72] K. P. Kolhe and C. K. Datta, "Prediction of microstructure and mechanical properties of multipass SAW," J. Mater. Process. Technol., vol. 197, no. 1-3, pp. 241-249, 2008, doi: 10.1016/j.jmatprotec.2007.06.066.

[73] J. Y. Choi, S. W. Hwang, and K. T. Park, "Twinning-induced plasticity aided high ductile duplex stainless steel," Metall. Mater. Trans. A Phys. Metall. Mater. Sci., vol. 44, no. 2, pp. 597-601, 2013, doi: 10.1007/s11661-012-1579-5.

[74] H. Gholizadeh, "The Influence of Alloying and Temperature on the Stacking-fault Energy of Iron-based Alloys," *PhD Diss. Mont. Leoben*, no. May, p. 193 pp., 2013.

[75] B. G. Prusty and A. Banerjee, "Structure-property correlation and constitutive description of structural steels during hot working and strain rate deformation," *Materials (Basel).*, vol. 13, no. 3, 2020, doi: 10.3390/ma13030556.

[76] F. Tehovnik, B. Arzenšek, B. Arh, D. Skobir, B. Pirnar, and B. Žužek, "Microstructure evolution in SAF 2507 super duplex stainless steel," Mater. Tehnol., vol. 45, no. 4, pp. 339-345, 2011.

[77] H. Li *et al.*, "Deformation Characteristic and Constitutive Modeling of 2707 Hyper Duplex Stainless Steel under Hot Compression," *Metals (Basel).*, vol. 6, no. 9, p. 223, 2016, doi: 10.3390/met6090223.

[78] D. Samantaray, V. Kumar, a K. Bhaduri, and P. Dutta, "Microstructural Evolution and Mechanical Properties of Type 304 L Stainless Steel Processed in Semi-Solid State," Int. J. Metall. Eng., vol. 2, no. 2, pp. 149-153, 2013, doi: 10.5923/j.ijmee.20130202.06.

[79] J. Humphreys, G. S. Rohrer, and A. Rollett, *Recrystallization and Related Annealing Phenomena: Second Edition*. 2017.

[80] C. P. Wang, F. G. Li, W. Lei, and H. J. Qiao, "Review on modified and novel techniques of severe plastic deformation," Sci. China Technol. Sci., vol. 55, no. 9, pp. 2377-2390, 2012, doi: 10.1007/s11431-012-4954-y.

[81] R. Jacob, S. Raman Sankaranarayanan, and S. P. Kumaresh Babu, "Recent advancements in manganese steels-A review," Mater. Today Proc., vol. 27, pp. 2852-2858, 2019, doi: 10.1016/j.matpr.2020.01.296.

[82] M. Sabzi and M. Farzam, "Hadfield manganese austenitic steel: A review of manufacturing processes and properties," *Mater. Res. Express*, vol. 6, no. 10, 2019, doi: 10.1088/2053-1591/ab3ee3.

[83] R. Hadfield, "HADFIELD'S MANGANESE STEEL.," Science, vol. 12, no. 306, pp. 284-286, Dec. 1888, doi: 10.1126/science.ns-12.306.284-a.

[84] L. Rémy and A. Pineau, "Twinning and strain-induced f.c.c. → h.c.p. transformation on the mechanical properties of CoNiCrMo alloys," Mater. Sci. Eng., vol. 26, no. 1, pp. 123-132, 1976, doi: 10.1016/0025-5416(76)90234-2.

[85] O. Bouaziz, H. Zurob, B. Chehab, J. D. Embury, S. Allain, and M. Huang, "Effect of chemical composition on work hardening of Fe-Mn-C TWIP steels," Mater. Sci. Technol., vol. 27, no. 3, pp. 707-709, 2011, doi: 10.1179/026708309X12535382371852.

[86] S. Allain, J. P. Chateau, O. Bouaziz, S. Migot, and N. Guelton, "Correlations between the calculated stacking fault energy and the plasticity mechanisms in Fe-Mn-C alloys," *Mater. Sci. Eng. A*, vol. 387-389, no. 1-2 SPEC. ISS., pp. 158-162, 2004, doi: 10.1016/j.msea.2004.01.059.

[87] Z. C. Yanushkevich, D. A. Molodov, A. N. Belyakov, and R. O. Kaibyshev, "Recrystallization kinetics of an austenitic high-manganese steel subjected to severe plastic deformation," Russ. Metall., vol. 2016, no. 9, pp. 812-819, 2016, doi: 10.1134/S0036029516090184.

[88] W. Yan, L. Fang, K. Sun, and Y. Xu, "Effect of surface work hardening on wear behavior of Hadfield steel," *Mater. Sci. Eng. A*, vol. 460-461, pp. 542-549, 2007, doi: https://doi.org/10.1016/j.msea.2007.02.094.

[89] M. Soleimani, A. Kalhor, and H. Mirzadeh, "Transformation-induced plasticity (TRIP) in advanced steels: A review," *Mater. Sci. Eng. A*, vol. 795, no. August, 2020, doi: 10.1016/j.msea.2020.140023.

[90] S. Sevsek, C. Haase, and W. Bleck, "Strain-rate-dependent deformation behavior and mechanical properties of a multi-phase medium-manganese steel," *Metals (Basel).*, vol. 9, no. 3, 2019, doi: 10.3390/met9030344.

[91] M. Bahramyan, R. T. Mousavian, and D. Brabazon, "Study of the plastic deformation mechanism of TRIP-TWIP high entropy alloys at the atomic level," *Int. J. Plast.*, vol. 127, no. June 2019, p. 102649, 2020, doi: 10.1016/j.ijplas.2019.102649.

[92] F. Javadzadeh Kalahroudi, H. Koohdar, H. R. Jafarian, Y. Haung, T. G. Langdon, and M. Nili-Ahmadabadi, "On the microstructure and mechanical properties of an Fe-10Ni-7Mn martensitic steel processed by high-pressure torsion," *Mater. Sci. Eng. A*, vol. 749, no. January, pp. 27-34, 2019, doi: 10.1016/j.msea.2019.02.002.

[93] H. Fu *et al.*, "Dynamic behaviors and microstructure evolution of iron–nickel based ultra-high strength steel by SHPB testing," *Metals (Basel).*, vol. 10, no. 1, 2020, doi: 10.3390/met10010062.

[94] L. S. Toth *et al.*, "Modeling the effect of primary and secondary twinning on texture evolution during severe plastic deformation of a twinning-induced plasticity steel," *Materials (Basel).*, vol. 11, no. 5, 2018, doi: 10.3390/ma11050863.

[95] M. C. Somani and L. P. Karjalainen, "Innovative Approaches in Physical Simulation and Modeling for Optimal Design and Processing of Advanced High Strength Steels," Mater. Manuf. Process., vol. 25, no. 1-3, pp. 133-141, 2010, doi: 10.1080/10426910903158223.

[96] J. H. Ryu, P. H. K. D. H. Bhadeshia, and P. D.-W. Suh, "Hydrogen Embrittlement in TRIP and TWIP Steels," *Grad. Inst. Ferr. Technol.*, vol. Ph.D., 2012.

[97] G. Frommeyer, U. Brüx, and P. Neumann, "Supra-ductile and high-strength manganese-TRIP/TWIP steels for high energy absorption purposes," ISIJ Int., vol. 43, no. 3, pp. 438-446, 2003, doi: 10.2355/isijinternational.43.438.

[98] J. Y. Kang, J. G. Kim, S. K. Kim, K. G. Chin, S. Lee, and H. S. Kim, "Outstanding mechanical properties of high-pressure torsion processed multiscale TWIP-cored three layer steel sheet," Scr. Mater., vol. 123, pp. 122-125, 2016, doi: 10.1016/j.scriptamat.2016.06.009.